

VARIATIONAL ASSIMILATION OF TAO AND XBT
DATA IN THE HOPE OGCM, ADJUSTING THE
SURFACE FLUXES IN THE TROPICAL OCEAN

Hans Bonekamp

Geert Jan van Oldenborgh

Gerrit Burgers

Royal Netherlands Meteorological Institute

NL-3730 AE De Bilt, Netherlands.

(e-mail: bonekamp@knmi.nl)

Manuscript: January 11, 2001

Abstract

A four-dimensional variational method has been developed that assimilates XBT and TAO sub-surface temperature data into the Hamburg Ocean Primitive Equation model. The method decreases the misfit between model and observed ocean temperatures by adjusting the surface forcing. The main goal of the assimilation scheme is to improve ocean analyses in the tropical Pacific. As a first study, only wind stress is adjusted in the assimilation. In two identical-twin experiments it is demonstrated that the scheme works well in the equatorial Pacific. The scheme is capable to reduce errors in the ocean analysis which originate either from the wind-stress forcing or the initial state. The impact of model errors on the data assimilation is investigated in an experiment with real observations. In this experiment, the temperature innovations near the equator are comparable to those of an Optimal Interpolation data-assimilation scheme.

1 Introduction

Currently more than a decade of high-quality observations of the tropical Pacific is available. Most of the subsurface observations originate from the Tropical Atmosphere Ocean (TAO) array of moored buoys, which has been set up during the Tropical Ocean Global Atmosphere (TOGA) program [WCRP, 1985] and from the expendable bathythermographs (XBT) measurements made by voluntary observing ships (VOS). These data have given an important contribution to the knowledge of the intra-seasonal and interannual variability in the tropical Pacific ocean [McPhaden *et al.*, 1998]. For example, using the TAO and XBT data, McPhaden [1999] monitored the evolution of the strong El Niño of 1997/1998 down to an ocean depth of 500 meter.

The availability of these observational data has given rise to a large number of ocean data-assimilation studies for the tropical Pacific [e.g. Malanotte-Rizzoli, 1996; Anderson *et al.*, 1996]. The aim of these studies is to provide more accurate ocean analyses, which are essential for the prediction of the large-scale, seasonal and interannual (ENSO) variations in the coupled atmosphere ocean system [Ji and Leetma, 1997; Stockdale *et al.*, 1998]. Relatively simple ocean models [e.g. Zebiak and Cane, 1987] describe the most relevant physics (which is only weakly nonlinear) reasonably well. Therefore, early studies combined simple ocean models with various data-assimilation methods, ranging from simple nudging methods [Zebiak and Cane, 1987] to advanced, computationally expensive data-assimilation methods like the four-dimensional variational data assimilation (4DVAR) [Sheinbaum and Anderson, 1989; Weaver and Anderson, 1996] and the Ensemble Kalman Filter [Cane *et al.*, 1996]. At present, several operational centres use complex Ocean General Circulation Models (OGCMs), which are more realistic, for their experimental seasonal forecasts. So far, these models have been combined with data-assimilation methods of moderate complexity [e.g. Alves *et al.*, 1998; Behringer *et al.*, 1998]. Yet, the best results are expected from combining OGCMs with advanced data-assimilation methods [e.g. Weaver and Vialard, 1999]. In the present paper, we consider a 4DVAR method for the Hamburg Ocean Primitive Equation model (HOPE) OGCM [Wolff *et al.*, 1997].

An important issue in four-dimensional ocean data assimilation is what kind of control over the model simulation should be used to achieve the best possible improvements in the ocean analysis. Given a four-dimensional data-assimilation method for an ocean model and a set of observations, the analysis depends on the initial model state and the surface forcing. To improve the analysis, most ocean 4DVAR schemes put their controls on the initial state only and the surface forcing is assumed to be perfect. This is a straightforward extension of previously employed three-dimensional variational or Optimal Interpolation (OI) methods. This approach has been useful [Sheinbaum and Anderson, 1989; Weaver and An-

erson, 1996; *Weaver and Vialard*, 1999], but it also has its drawbacks and difficulties. Firstly, the surface forcing is in fact poorly known [*Miller and Cane*, 1996] particularly in the western equatorial Pacific. In this area, the air-sea interaction is strongly influenced by moist convection. This is relatively poorly represented in Atmospheric General Circulation Models, which determine flux fields from properties at and near the sea surface. Therefore, the assumption of a perfect surface forcing is not realistic. Secondly, additional constraints and smoothing must be added to keep updates of the initial state physically realistic and to suppress unwanted initialization shocks. Thirdly, in non-eddy-resolving OGCMs the impact of an adjusted initial state on the ocean analysis decays in time. So, for longer assimilation periods unrealistically large adjustments are often required to obtain a correction in the ocean analysis with the right amplitude.

In this study, we have implemented a global 4DVAR data assimilation scheme in which the surface forcings are the control variables. A weak constraint keeps the surface forcing close to a realistic background value. Controlling the surface forcing has several advantages. Firstly, an important advantage is the gradual adjustment of the prognostic fields (e.g. salinity and temperature) that is consistent with the ocean-model equations. Secondly, longer assimilation periods make sense because the effect of improved forcings on the ocean analysis is integrated by the model rather than dissipated. However, the effective assimilation period will still be limited by model errors. Thirdly, the adjusted surface forcing is an alternative surface-flux product which can be used for intercomparison studies [e.g. *Tziperman and Bryan*, 1993; *Yu and O'Brien*, 1995]. Finally, the dimension of the variational problem can be kept fairly small because the surface forcing is made up from two-dimensional fields.

The scheme uses a strong constraint for the ocean-model equations. In a weak model constraint approach the effects of model errors would be accounted for by allowing corrections to the model trajectory. In our case, some model errors can be compensated for by wind stress corrections.

The set-up of the 4DVAR scheme is global and for all type of surface forcings, but we focus in this first study on the adjustment of tropical Pacific wind stresses. We assimilate the ocean temperature measurements of the TAO buoy array and XBTs along major ship routes. We use the HOPE OGCM version described in *Stockdale* [1997]. This model is employed as the ocean component of the seasonal forecast system of the European Centre for Medium Range Weather Forecasts (ECMWF). Its adjoint, which is required to solve the variational problem, is documented in *van Oldenborgh et al.* [1999]. The model forcing is based on the daily air-sea fluxes of the ECMWF Operational Analysis (EOA). The wind stress is corrected in the assimilation process but the heat and freshwater flux are applied as given. The sea surface salinity and temperature are relaxed towards the *Levitus* [1982] climatology and *Reynolds and Smith* [1995] observations, re-

spectively. The latter relaxation is chosen to be very strong, which means that the effective heat flux is determined by the observed sea surface temperature.

The ultimate goal of the 4DVAR scheme is to improve ocean analyses for seasonal predictions with a coupled atmosphere-ocean system. However, first the efficacy of the 4DVAR scheme and the usefulness of the analyses have to be demonstrated in both experimental and realistic settings. Therefore, in this paper, we address the following basic questions. Is the 4DVAR scheme capable of improving the ocean model trajectory? Can we make a quantitative or qualitative statement about the usefulness of the ocean analysis at the end of the assimilation period?

To find answers to these questions we have performed three numerical experiments. Two of these are of the identical-twin type and one considers real observations. In the identical-twin experiments, the defined ‘truth’ is an unperturbed HOPE model run with EOA wind stress. During this run pseudo-observations are generated, which are the model counterparts from this run at the actual TAO buoy and XBT measurements. In the first identical-twin experiment, a ‘first-guess’ wind stress is constructed by perturbing the EOA wind stress. In the second, perturbations are added to the initial state, not to the wind stress. In this way, the effects of forcing and initial state errors can be studied separately. The last experiment is done with real observations. In this case, model errors can hamper the functioning of the 4DVAR method. Indications of a proper convergence of the cost are analyzed and the features of the ocean analysis are assessed qualitatively. In addition, the ocean analysis is compared with that of the OI scheme that is used in seasonal forecasting at the ECMWF [Alves *et al.*, 1998].

The outline of the paper is as follows. In section 2 we briefly describe the HOPE model and the observational data. Section 3 contains a formulation of the variational problem and the data assimilation scheme. The identical twin experiments and their results are presented in section 4. The experiment with real observations follows in section 5. We discuss our results in section 6 and, finally, the conclusions are summarized in section 7.

2 Model and Data

2.1 The HOPE Model

The Ocean General Circulation Model (OGCM) used in this study is the Hamburg Ocean Primitive Equation Model (HOPE). Details of the model physics and the applied numerical scheme are described by Wolff *et al.* [1997]. The global version used here is that of the ECMWFs Seasonal Forecast Project [Stockdale, 1997]. The horizontal resolution varies from 0.5° meridionally by 2.8° zonally

near the equator to 2.8° by 2.8° in the mid-latitudes. In the vertical, 10 levels are placed in the top 300 meters and another 10 levels cover the deep ocean. Discretization is on an Arakawa E-grid and the integration time step equals 2 hours. The model contains a realistic bottom topography and a free surface. No sea ice model is included. Northward of 60°N and southward of 60°S the prognostic fields of velocity, salinity and temperature are relaxed towards the *Levitus* [1982] climatology.

The model is forced with surface fluxes (heat, freshwater and momentum) from the ECMWF Operational Analysis. These fields are interpolated from an T42 spectral resolution to a regular 2.8° by 2.8° grid. The solar radiation affects the top model levels. A very strong Newtonian relaxation ($\lambda = 400 \text{ Wm}^{-2}\text{K}^{-1}$) is applied to keep the model SST close to the observed data set of *Reynolds and Smith* [1995]. The fresh water flux consists of precipitation minus evaporation plus the run-off of the world's major rivers.

In the 4DVAR optimization the adjoint of the HOPE model (adHOPE) is used. This adjoint model has been developed for the full model equations. An description of AdHOPE is given in *van Oldenborgh et al.* [1999]. Backward integrations of this model gives the gradient of cost function with respect to control over the surface forcing (see section 3).

2.2 XBT and TAO data

The observational data used in this study are the subsurface temperature measurements by the TAO array, by the expendable bathythermographs (XBT) from voluntary observing ships (VOS), and by several other buoys in the tropical Pacific. The TAO array consists of nearly 70 ATLAS moorings spanning the width of the equatorial Pacific Ocean. The VOS take measurements along 18 specific lines which cross the equator at different longitudes. A more detailed description of these observational data can be found in e.g. *McPhaden et al.* [1998]. We use the quality control of the ECMWF Seasonal Forecast Project [*Alves et al.*, 1998] to select the observations for assimilation.

Figure 1 shows the number of assimilated temperature measurements for a typical eight-week period. Clearly, most observations originate from the TAO array. As a result, the equatorial region (10°S to 10°N) is much better sampled than the off-equatorial regions.

3 The Variational Data Assimilation Scheme

The 4DVAR data assimilation method used in this study attempts to minimize a cost function J that quantifies the misfit between model temperatures and observations. It is made up from a background term for the forcing and an observational

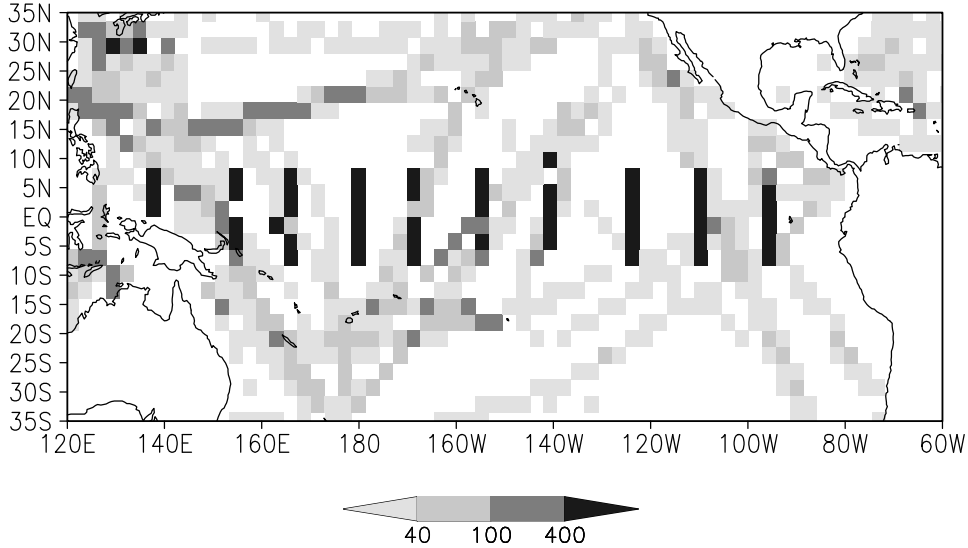


Figure 1: Number of assimilated observations per $2.8^\circ \times 2.8^\circ$ grid box in the 8-week period February 12, 1995 to April 9, 1995. Note the logarithmic scale.

term for the temperature misfits ,

$$J(\mathbf{c}) = J_{\text{bg}}(\mathbf{c}) + J_{\text{obs}}(\mathbf{c}) = \mathbf{c}^T \mathbf{B}^{-1} \mathbf{c} + (\mathbf{H}\mathbf{x}(\mathbf{c}, \mathbf{x}_0) - \mathbf{z})^T \mathbf{E}^{-1} (\mathbf{H}\mathbf{x}(\mathbf{c}, \mathbf{x}_0) - \mathbf{z}). \quad (1)$$

The vector \mathbf{c} contains the control parameters, in this case a parameterization of the wind stress. The vector \mathbf{x} contains the HOPE model trajectory, and \mathbf{z} the ocean temperature measurements during an eight-week assimilation time window. The first term J_{bg} is the background term and \mathbf{B} is the covariance matrix of the errors in wind stress. This term penalizes for too strong deviations from the prescribed background forcing; for $\mathbf{c} = 0$ the first-guess forcing is employed.

The second term J_{obs} is the observation term. It is the sum of the quadratic misfits between observed and modeled temperature values during the assimilation time. The model temperature output depends on the initial state \mathbf{x}_0 and the control vector \mathbf{c} . \mathbf{H} is the observation operator which projects the model output on the model counterpart of the observational data. \mathbf{E} is the observational error covariance matrix which accounts both for the errors in the measurements and the projection \mathbf{H} . In the remainder of this section we will discuss the various aspects of the cost function in further detail.

3.1 Wind Stress Variations

In the experiments wind stress is used as control variable. The following scale consideration has been made for the temporal resolution of wind-stress updates. Typical scales of weather systems, upper ocean temperature anomalies, and buoy distances are in the order of 1000 km. The fastest subsurface temperature adjustments in the upper ocean are by equatorial Kelvin waves, which propagate at approximately 3 ms^{-1} . Hence, the upper ocean is sensitive to wind-stress variations in the order of one week or longer only. Therefore, we use a two-weekly variation of the wind stress; the wind-stress forcing is determined as the sum of a first-guess wind stress $\boldsymbol{\tau}_i^{\text{fg}}$ and a linear interpolation (in time) of 2 two-weekly wind-stress corrections $\boldsymbol{\tau}_j^{\text{corr}}$.

$$\boldsymbol{\tau}_i = \boldsymbol{\tau}_i^{\text{fg}} + \alpha_i \boldsymbol{\tau}_j^{\text{corr}} + (1 - \alpha_i) \boldsymbol{\tau}_{j+1}^{\text{corr}}. \quad (2)$$

Index j is chosen such that the pair $(\boldsymbol{\tau}_j^{\text{corr}}, \boldsymbol{\tau}_{j+1}^{\text{corr}})$ brackets the ocean model time step (index i) and $\alpha_i = (t_{j+1} - t_i)/(t_{j+1} - t_j)$.

The control vector \mathbf{c} is made up of the time sequence of $(m + 1)$ wind stress corrections from the beginning to the end of the assimilation window

$$\mathbf{c} = (\boldsymbol{\tau}_0^{\text{corr}} | \boldsymbol{\tau}_1^{\text{corr}} | \dots | \boldsymbol{\tau}_m^{\text{corr}}). \quad (3)$$

As a consequence of this set up, the assimilation time window must be taken as a multiple of 14 days. In our applications, we have taken $m = 4$, so that the control vector contains 5×2 two-dimensional forcing fields.

3.2 Error Covariances and Preconditioning

The performance of the 4DVAR scheme strongly depends on the specification of the background error covariance matrix \mathbf{B} (see equation 1). On the one hand, it determines the importance of J_{bg} relative to J_{obs} . On the other hand, it determines the effective dimension of the minimization problem. In general, the elements of \mathbf{B} , the (co)variances of the errors in two-weekly wind stress, are unknown and have to be estimated from a motivated guess.

In a first approach, we make two simplifying assumptions which could be replaced with more realistic approximations in later studies. The first is to neglect any time dependence in the covariances. As a consequence, \mathbf{B} has a block structure which is based on the index j (see subsection 3.1) and a sub-matrix with the spatial error covariances between the ocean points (x, y) and (x', y') . These covariances are denoted by $\beta(x, y; x', y')$. The second is to assume that errors in τ_x and τ_y are uncorrelated. This implies that the spatial error covariances of τ_x and τ_y can be estimated separately.

The next issue is to obtain plausible estimates of the spatial error co-

variances $\beta(x, y; x', y')$. This problem can be split up in estimating the correlations $\rho(x, y; x', y')$ and the standard deviations $\sigma(x, y)$, since $\beta(x, y; x', y') = \sigma(x, y)\sigma(x', y')\rho(x, y; x', y')$. We expect that the correlations in the wind stress error decreases rapidly and smoothly with the distance between the points (x, y) and (x', y') . A common and theoretically convenient way to meet this expectation is to assume that $\rho(x, y; x', y')$ has a Gaussian shape. Here, we presume a symmetric Gaussian shape with the main axes in the meridional and latitudinal direction

$$\rho(x, y; x', y') = \exp\left(-\frac{(x - x')^2}{2\lambda_x(x, y)\lambda_x(x', y')} - \frac{(y - y')^2}{2\lambda_y(x, y)\lambda_y(x', y')}\right). \quad (4)$$

Hence, \mathbf{B} can be parameterized in terms of $\sigma(x, y)$ and the zonal and meridional decorrelation lengths $\lambda_x(x, y)$ and $\lambda_y(x, y)$.

The parameters $\sigma(x, y)$, $\lambda_x(x, y)$ and $\lambda_y(x, y)$ are estimated from two-weekly wind-stress differences. In fact, we have taken two-weekly averaged wind-stress data of the ECMWF reanalysis (ERA)[*Gibson et al.*, 1997]. From these averages we have calculated two-weekly differences. Next, we have chosen $\sigma(x, y)$ to be 20% of the standard deviation in these differences and the decorrelation lengths $\lambda_x(x, y)$ and $\lambda_y(x, y)$ are determined by a fit of the distribution (4) to the correlations of these differences. The resulting $\sigma(x, y)$ ranges in the tropical Pacific for both τ_x and τ_y from 0.001 Nm^{-2} to 0.011 Nm^{-2} . Figure 2 shows the spatial map of $\lambda_x(x, y)$ for τ_x differences to illustrate the decorrelation lengths. $\lambda_x(x, y)$ for τ_x ranges roughly from 12° to 25° which corresponds to 4 and 9 forcing grid boxes, respectively. $\lambda_x(x, y)$ for τ_y has the same order of magnitude. The $\lambda_y(x, y)$ are approximately a factor 2 smaller for both τ_x and τ_y .

It is important to note that the effective dimension of the minimization problem is reduced by the smoothness implied by this choice of \mathbf{B} . On the basis of the correlation lengths we estimate this dimension to be about 50 variables per forcing field over the Tropical Pacific.

For large dimensions, direct inversion of \mathbf{B} is computationally prohibitive. We can circumvent this inversion with a pre-conditioning [*Courtier et al.*, 1994] of the variational problem as follows. With the decomposition $\mathbf{B} = \mathbf{A}\mathbf{A}^T$ and the transformation

$$\mathbf{c} = \mathbf{A}\mathbf{d} \quad (5)$$

the background term can simply be written as $J_{\text{bg}} = \mathbf{d}^T\mathbf{d}$. Moreover, with $J_{\text{obs}}(\mathbf{c}) = J_{\text{obs}}(\mathbf{A}\mathbf{d})$, equation (1) can be minimized as a function of the vector \mathbf{d} rather than \mathbf{c} .

The challenge is then to calculate the transformation \mathbf{A} . First we separate

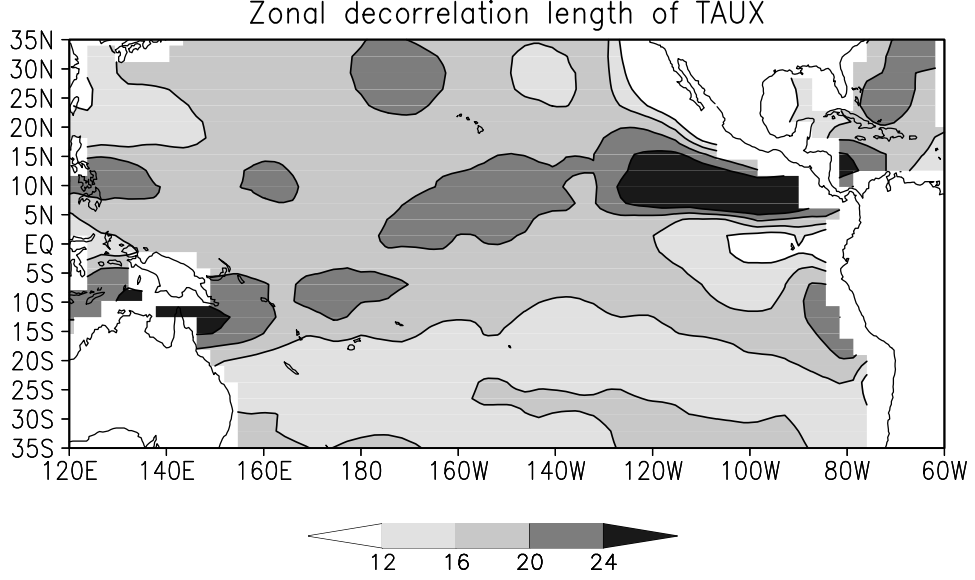


Figure 2: The zonal decorrelation length $l_x(x, y)$ (in degrees) of two-weekly zonal wind stress differences.

the contributions of $\sigma(x, y)$ and $\rho(x, y; x', y')$ in \mathbf{A} as follows,

$$\mathbf{A} = \mathbf{S}\mathbf{L}, \quad (6)$$

with $\mathbf{S} = [\sqrt{\sigma(x, y)\sigma(x', y')}]$ and $\mathbf{L}\mathbf{L}^T = [\rho(x, y; x', y')]$. An exact method to calculate \mathbf{c} from \mathbf{d} would be to obtain explicit expression of \mathbf{L} . Here we use a computationally efficient approximation for the transformation \mathbf{L} that is valid for slowly varying decorrelation lengths. When λ_x and λ_y are constant the elements of the vector $\mathbf{L}\mathbf{d}$ can be written as a discretized evaluation of the continuous convolution

$$\iint dx' dy' \psi(x, y; x', y') d(x', y'), \quad (7)$$

with

$$\psi(x, y; x', y') = \exp\left(-\frac{(x-x')^2}{\lambda_x^2} - \frac{(y-y')^2}{\lambda_y^2}\right). \quad (8)$$

This approximation is exact for an infinitely high resolution and an infinite do-

main. Next, the convolution (7) is evaluated by means of the diffusion process

$$4\frac{\partial u}{\partial s} = \lambda_x^2 \frac{\partial^2 u}{\partial x^2} + \lambda_y^2 \frac{\partial^2 u}{\partial y^2}, \quad (9)$$

see e.g. *Egbert et al.* [1994]. This equation has the general solution

$$u(x, y, s) = \frac{1}{2\pi s \lambda_x \lambda_y} \iint dx' dy' \psi(x, y; x', y') u(x', y', 0). \quad (10)$$

Thus, we can obtain transformation \mathbf{A} (see equation 5) by solving the diffusion equation (9). Vector \mathbf{d} must be taken as the initial condition ($s = 0$) and \mathbf{c} is obtained from a multiplication of the solution for $s = 1$ with the normalization factor ($2\pi\lambda_x\lambda_y$) and with matrix \mathbf{S} . In this study, we make a further approximation, because we solve equation (9) but with the $\lambda_x = \lambda_x(x, y)$ and $\lambda_y = \lambda_y(x, y)$ from the described Gaussian fit to the ERA wind stress differences. The numerical evaluation is done with a common finite difference method.

An important advantage of the diffusion equation approach over an exact evaluation of \mathbf{A} is the straightforward treatment of the lateral ocean boundaries. The error correlations are ‘diffused’ against these boundaries as if they were solid walls. Consequently, errors in wind stress over different basins (e.g. the Pacific and the Atlantic basin) are uncorrelated. Another advantage of this approach is that it results in smoother error covariances, which is beneficial for the optimization of J .

Finally, we discuss the second term of the cost function, J_{obs} . This term is determined by the observation operator \mathbf{H} and observation error covariances \mathbf{E} . In this study, \mathbf{H} is a linear interpolation from the Arakawa E grid of the potential temperature to the position of the observation. The even and odd grid are interpolated individually and weighted equally. In time, the observations are assigned to the nearest ocean-model time step (every 2 hours). The HOPE model uses potential temperature as a prognostic variable. Therefore, \mathbf{H} contains a conversion to regular temperatures based on the experimental formula of *Bryden* [1973].

The dimension of \mathbf{E} equals the number of observations during the assimilation window. Errors in the observations are assumed to be spatially and temporally uncorrelated. Therefore, the matrix \mathbf{E} and its inverse have a diagonal structure. In the identical twin experiments (section 4) that have perfect pseudo-observations, the temperature error is chosen to be 0.3 K for the XBTs, the TAO and the other buoy data. This is a rough estimate of the interpolation error. For the real-observation experiment (section 5) this value is increased to 1.0 K. This value is the lowerbound of the range that has been used by *Behringer et al.* [1998]

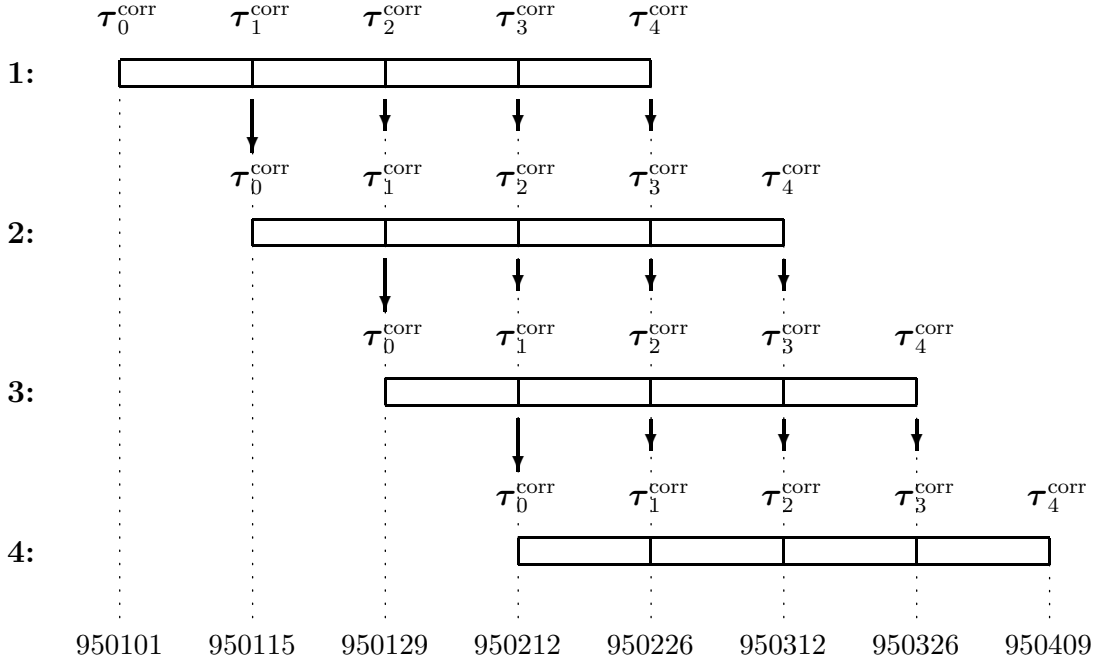


Figure 3: Schematic diagram of 4 assimilation cycles. Time is from left to right. The re-use of the two-weekly wind-stress corrections from the previous assimilation window is indicated by the arrows. In addition, the long arrows mark the re-use of the model state as the initial state of the next assimilation window.

to scale the temperature variances resulting from ocean-model errors.

3.3 Set-up of the Numerical Experiments

We have set up our numerical experiments in such a way that they simulate an operational forecasting cycle (see Figure 3). Each experiment starts from a given initial state at t_0 , here January 1, 1995. A first-guess model trajectory is then generated by integrating the model forward in time for a period of eight weeks. This model trajectory and the (pseudo)observations are used to make a first evaluation of the cost function J . This value of J reflects the misfit between the first-guess (background) model trajectory and the (pseudo)observation, since the wind-stress corrections are still zero. From here we calculate a best-guess trajectory by constructing the five wind stress corrections (τ_i^{corr} , $i = 0, 4$) that minimize J .

Technically, the minimization is done with the Quasi-Newton routine M1qn3 of the MODULOPT library [Gilbert and Lemaréchal, 1989]. The required evalu-

ations of the gradient ($\partial J/\partial \mathbf{d}$) are obtained from backward integration with ad-HOPE. These integrations are computationally expensive, approximately 5 times a forward HOPE run. This constraints the allowable number of iterations with M1qn3. In all the experiments, the maximum number of iterations has been set to six.

After the first period of eight weeks is dealt with, we repeat the assimilation cycle with a time window shifted by two weeks, see Figure 3. As initial state the best-guess estimate (analysis) at $t = t_1$ of the first cycle is taken, and for the first 6 weeks the best-guess updates ($\boldsymbol{\tau}_i^{\text{corr}}$, $i = 0, 3$) of the previous cycle are reused, whereas the new $\boldsymbol{\tau}_4^{\text{corr}}$ is set to zero. By this, the computational cost of a two-weekly analysis is about $5 \times 6 \times 4 = 120$ times a forward run over two weeks.

Each of our numerical experiments consists of four shifted assimilation runs, which we will denote as cycle 1, 2, 3 and 4. We will focus our discussion on, 1) the value of J (both as a function of cycle and iteration number and as a function of latitude), 2) the potential temperature fields at the end of cycle 4, which is at April 9, 1995, $4 \times 14 + 3 \times 14 = 98$ days later, and 3) the wind stress update at the beginning of cycle 4 (February 12, 1995). This update has been optimized through all four consecutive cycles.

4 Identical-twin Experiments

The 4DVAR scheme for the HOPE model has been tested in two identical-twin experiments. In these experiments we compare the results of two perturbed runs with those of a reference run (the ‘truth’ run, runT). The first perturbed run (the background run) is made without data assimilation and the second run (the analysis run) is made with assimilation of pseudo-observations.

In both the identical-twin experiments, runT is defined as a HOPE run without data assimilation. The initial state at January 1, 1995 is an ocean analysis that was created using the HOPE model and the OI scheme of the ECMWF’s seasonal forecasting group [Alves *et al.*, 1998]. The ECMWF Operational Analysis forcing is employed for 98 days. During this run pseudo-observations are collected. These are defined as projections of the model temperature at the locations and hours of the actual TAO buoy and XBT temperature measurements (see section 3.2)

$$\mathbf{z}^{\text{pseudo}} = \mathbf{H}\mathbf{x}(\mathbf{c}, x_0). \quad (11)$$

Thus, for runT both the observational term and the wind-stress term of the cost function (1) equal zero. As discussed in section 1, we will only consider perturbations in the tropical Pacific (35°S – 35°N). Accordingly, we include only

Experiment I: $J_{\text{obs}}/N_{\text{obs}}$

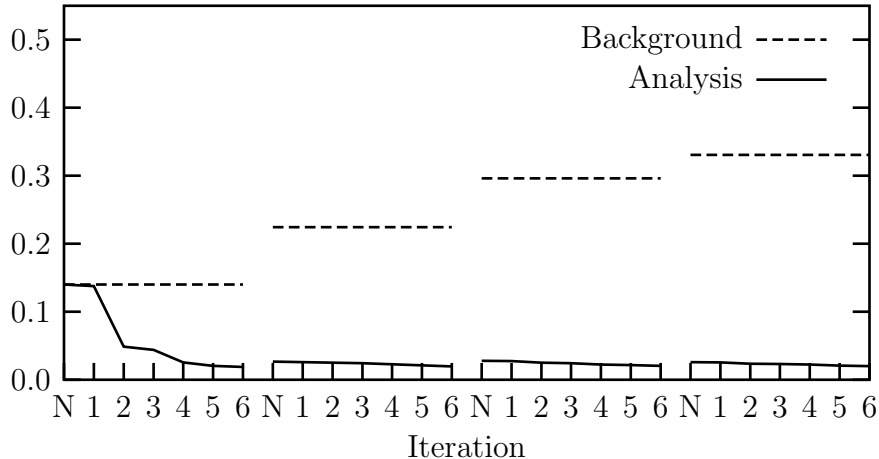


Figure 4: Experiment I. Convergence of $J_{\text{obs}}/N_{\text{obs}}$ as a function of iteration and assimilation cycle. N_{obs} is the number of observations in the assimilation window. The 4 cycles are the partly overlapping (see Figure 3) assimilation windows of 8 weeks. The solid (dashed) line represents the run with (without) data assimilation, which is runA1 (runBG1).

pseudo-observations in the region of 30°S to 30°N . The pseudo-observations are further restricted to below 10m to avoid interference with the SST relaxation.

4.1 Experiment I.

In this experiment, the wind-stress forcing in the tropical Pacific (35°S – 35°N) is perturbed to test the capability of the 4DVAR scheme to reduce resulting potential-temperature perturbation in the upper ocean and the forcing perturbation itself. Ideally, both the wind-stress and upper-ocean perturbation will be nullified. Yet, the cost cannot become exactly zero, because the background term J_{bg} will always have a positive value. The (perturbed) first-guess wind stress τ_i^{fg} is chosen as 80% of the original 1995 wind stress plus 20% of the 1996 wind stress in the tropical Pacific. In this way, the perturbation is large enough to have considerable impact on the upper ocean, but not so large to make the forcing unrealistic. In the areas 35°S – 25°S and 25°N – 35°N a lateral linear interpolation is used to match the first-guess to the true wind stress in a continuous way. For both background run (runBG1) and the analysis run (runA1), the initial state at January 1, 1995 is equal to that of the truth run. In runBG1 $\tau_i = \tau_i^{\text{fg}}$ is employed over the 98 days, while in runA1 this forcing is updated in the consecutive assimilation cycles.

First we compare the cost of the background and analysis run. The obser-

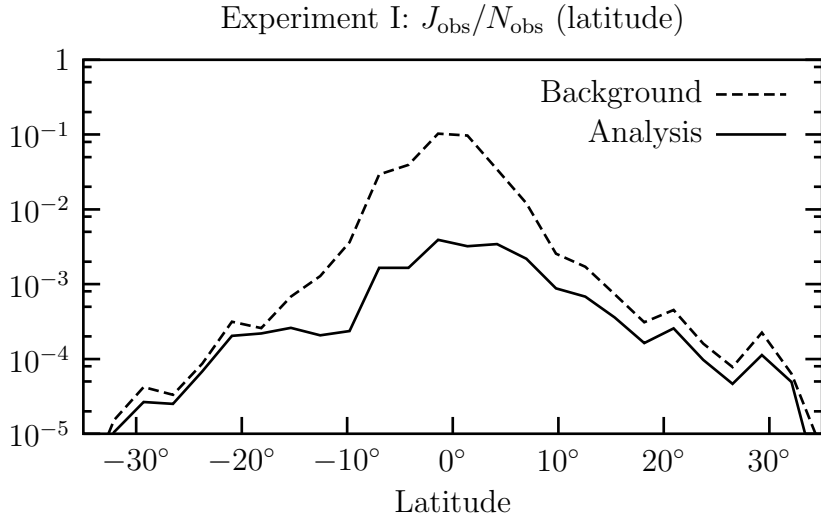


Figure 5: Experiment I. $J_{\text{obs}}/N_{\text{obs}}$ as a function of latitude on a logarithmic scale. N_{obs} is the number of observations in the assimilation window. Values are for the assimilation cycle 4, ending on April 9, 1995 (see Figure 3). The solid (dashed) line represents the run with (without) data assimilation, which is runA1 (runBG1).

vational cost of both runs is normalized with the number of observations (N_{obs}) in the assimilation window over which the cost function is defined. The results as a function of iteration and cycle are shown in Figure 4. In the initial cycle, data assimilation gives a big decrease in $J_{\text{obs}}/N_{\text{obs}}$ with most of the effect in the first 3 iterations. For the next 3 iterations convergence is slower. Shifting the assimilation window results in an increase of $J_{\text{obs}}/N_{\text{obs}}$ for runBG1, because the model state for January 15, 1995 has been perturbed already by τ^{fg} over the period January 1–14, 1995. However, for runA1 the increase in $J_{\text{obs}}/N_{\text{obs}}$ is much smaller, because the initial state is the runA1 analyzed state for January 15, 1995 and partly optimized wind stress are used over the first 6 weeks, see Figure 3. Subsequently, the 6 iterations of this assimilation cycle account for a small reduction of the $J_{\text{obs}}/N_{\text{obs}}$. The difference between runA1 and runBG1 is enlarged in the next 2 cycles in a similar manner.

The final (fourth assimilation cycle, ending on April 9, 1995) total cost of runA1 normalized with N_{obs} amounts to 0.025. This is a strong reduction when compared with the background value of 0.33. From Figure 5, it can be seen that the largest reductions are in the equatorial region (17°S – 12°N). The final total cost for runA1 is still for nearly 75% due to J_{obs} . In fact, the background term J_{bg} (not shown) remains less than quarter of J_{obs} throughout the assimilation. Figure 5 also shows that large contributions of the remaining costs are from the large number of observations in the equatorial region. The most likely reasons

for the remaining residuals are the coarse resolution of the wind-stress innovation and the short length of the assimilation window. These aspects will be discussed in more detail in section 6.

Next we compare the ocean analysis at April 9, 1995 of runA1 and runBG1 with that of runT. Figure 6 shows the difference in potential-temperature in the tropical Pacific at a depth of 100 m, along the equator, and along the 180°W meridian. The run with data assimilation (runA1) is much closer to the true ocean state (runT) than in the run without data assimilation (runBG). The largest improvements are obtained between -10°S and 10°N. For example, the large positive perturbation eastward of New Guinea has disappeared completely (see top panels of Figure 6). However, after data assimilation (top right panel) there are still some isolated, positive and negative anomalies in this region. In some cases the sign of these anomalies is opposite to that of the original perturbations (top left panel). This suggests that these anomalies might result from a too coarse resolution of the innovated wind stress which will be discussed in section 6.

In off-equatorial regions (35°S–15°S and 10°N–35°N), the potential temperature innovations are small, see Figure 6. For example, the positive perturbation near 25°N, 170°W, (top panels) remain in the order of magnitude of those of runBG1. The middle and bottom panels of Figure 6 demonstrate that the equatorial improvements go down to the depth of at least 240 m, which means that the errors induced by the wind-stress perturbations are strongly reduced in the complete equatorial wave guide.

Finally, we discuss the wind-stress innovation. Figure 7 shows the wind-stress perturbation with (middle panel) and without (top panel) data assimilation for the period February, 12–18 1995. For this week, the wind stress of runA1 has been updated in all 4 assimilation cycles. The plotted perturbations are averages weighted according to the linear interpolation of equation 2. The difference (runBG1-runA1) is depicted in the bottom panel. Near the equator (5°S–5°N), the data assimilation has recaptured most of the true wind stress. The differences are less than 0.005 Nm^{-2} (10%). The good performance in this region is in accordance with the results found for the ocean initial conditions in Figure 6. However, the off-equatorial wind-stress perturbations are hardly better with data assimilation. A positive exception is the north-western part of the warm pool area (northward of 5°N and westward of 150°E) with a reduction in wind-stress differences up to a factor two. In this area the number of observations is higher, see Figure 1.

4.2 Experiment II

In this identical-twin experiment it is attempted to compensate for perturbations in the initial state by a wind-stress update. An important question is, can the upper-ocean temperature misfits disappear with a wind-stress innovation that

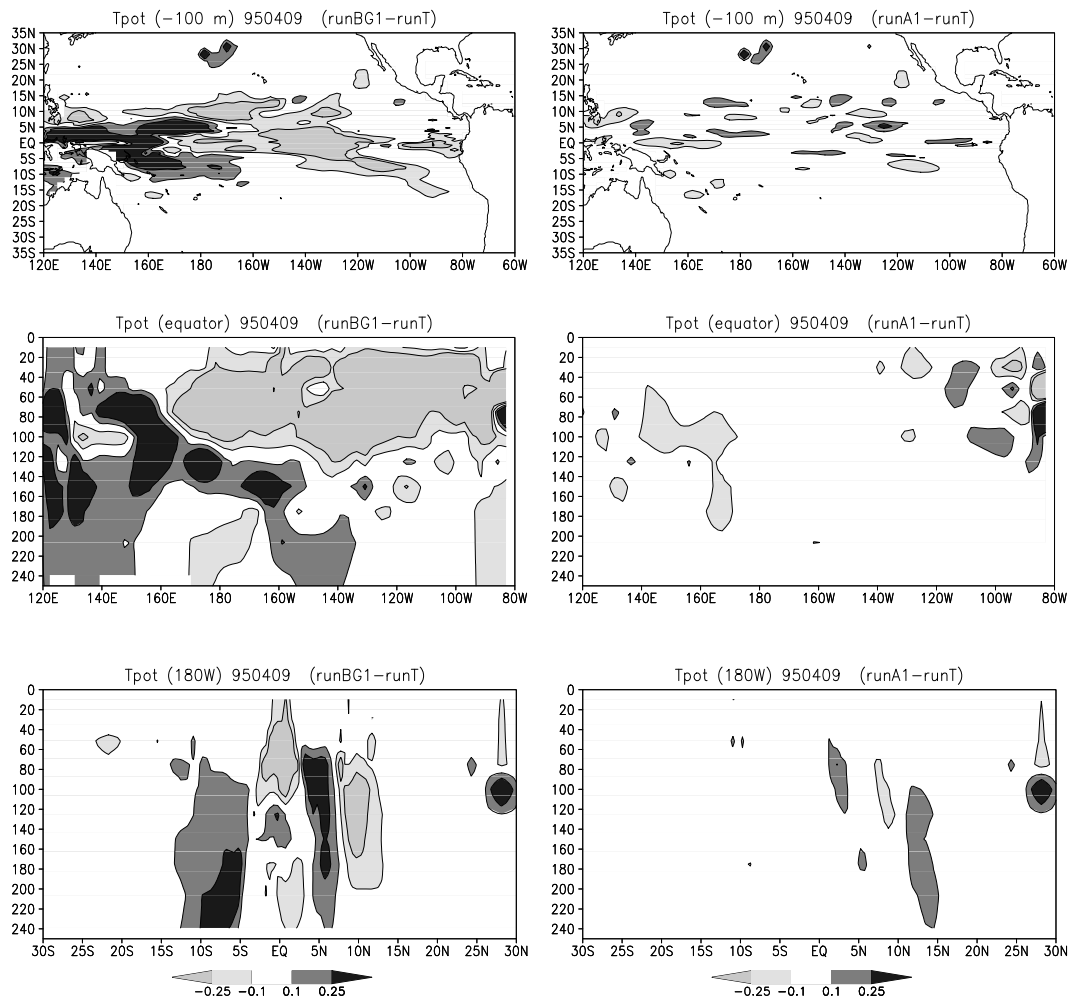


Figure 6: Experiment I: Potential temperature differences (K) at the end of assimilation cycle 4 (April 9, 1995). The differences are between (left panels) the background run and the truth run and (right panels) between the analysis run (runA1) and the truth run. The 100 m layer differences are in the top panels. The differences along the equator and the 180°W meridian are in the middle and bottom panels, respectively. Data of the top layer are not included.

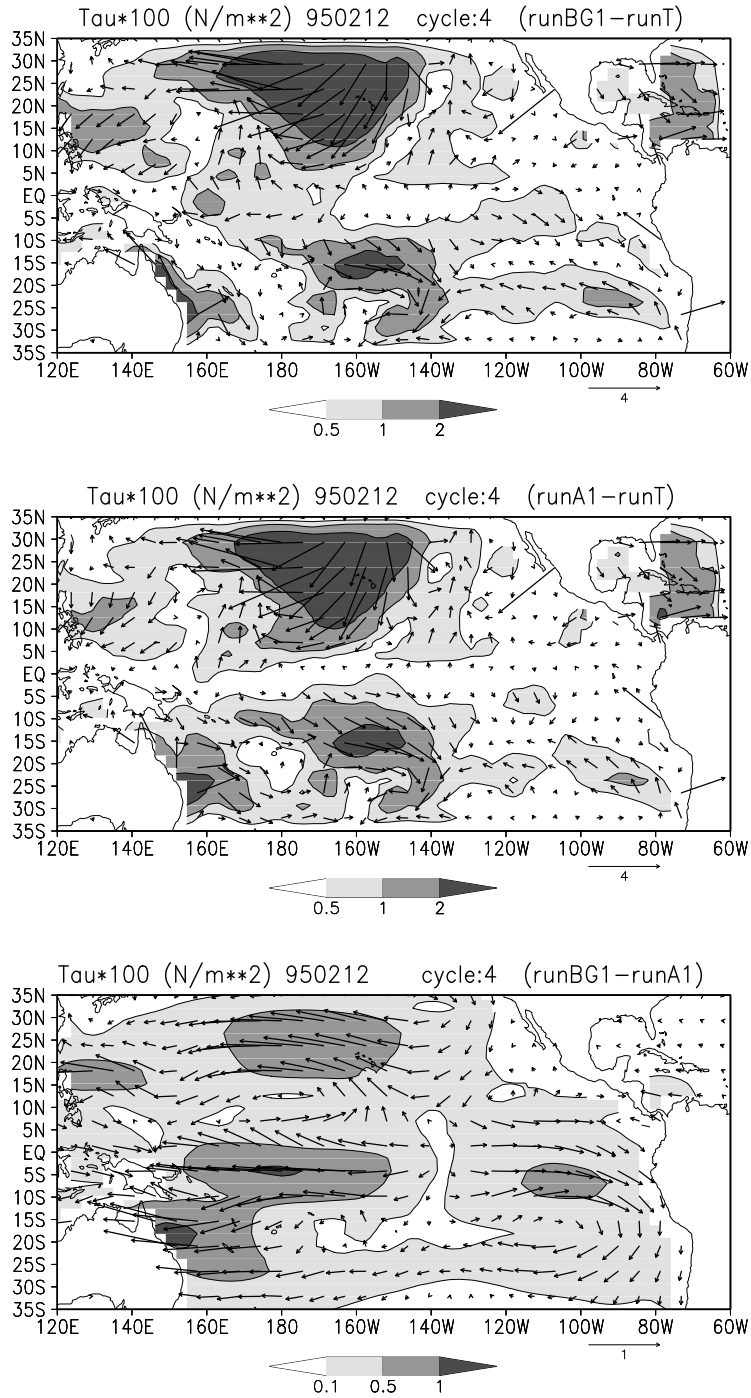


Figure 7: Experiment I: (Top panel) true wind-stress perturbation, (middle panel) wind-stress perturbation after assimilation, and (bottom panel) the wind-stress update. The plots are weighted time averages for the first week of the fourth assimilation cycle (February 12–18, 1995, see Figure 3). The weighting is according to the linear interpolation of equation 2. Note the different scaling of the bottom panel.

Experiment II: $J_{\text{obs}}/N_{\text{obs}}$

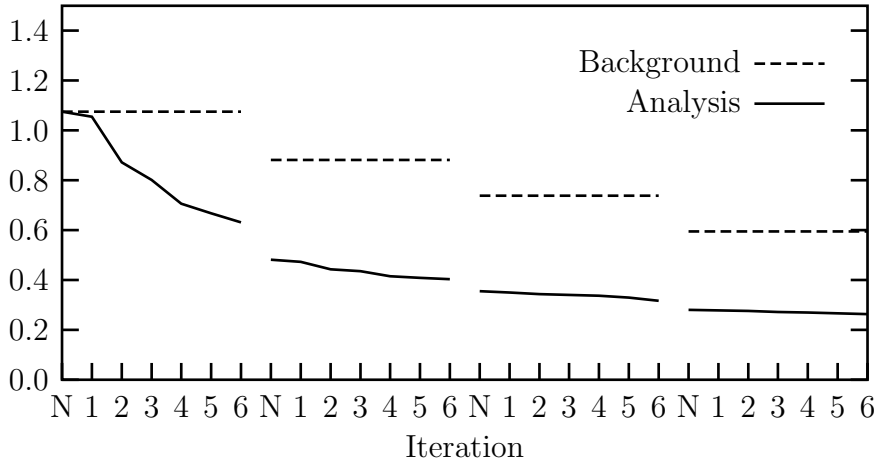


Figure 8: Experiment II. Convergence of $J_{\text{obs}}/N_{\text{obs}}$ as a function of iteration and assimilation cycle. N_{obs} is the number of observations in the assimilation window. The 4 cycles are the partly overlapping (see Figure 3) assimilation windows of 8 weeks. The solid (dashed) line represents the run with (without) data assimilation, which is runA2 (runBG2).

differs from the true wind stress within the order of the assumed error bound? A positive answer this question would mean that difficulties with updating the initial state (see section 1) can be circumvented.

The perturbed initial state is defined as 80% of the January 1, 1995 analyzed state (with the ECMWFs OI scheme) plus 20% of the state of January 1, 1996. In the areas 35°S – 25°S and 25°N – 35°N a lateral linear interpolation is used to match the perturbed with the true ocean state. The first-guess forcing τ_i^{fg} is the original EOA wind stress. Again, pseudo observations are used for the analysis run (runA2) and the output of this run is compared with that of runT and a first guess run (runBG2).

In this experiment, it is not realistic to expect that the initial-state perturbations can be nullified, because the upper-ocean perturbations are not the effect of a change in forcing.

First we discuss the cost function. In Figure 8 the convergence of $J_{\text{obs}}/N_{\text{obs}}$ for runA2 and runBG2 is shown. As in experiment I, the initial iterations of the first 2 assimilation cycles reduce most the costs of runA2. In contrast to experiment I, the cost of the first-guess run (runBG2) decreases at the shifts of the assimilation window due to a loss of memory of the initial-state perturbations. Nonetheless, runA2 is able to preserve a reduction with respect to runBG2 to the last assimilation window. This indicates an improved ocean analysis with data

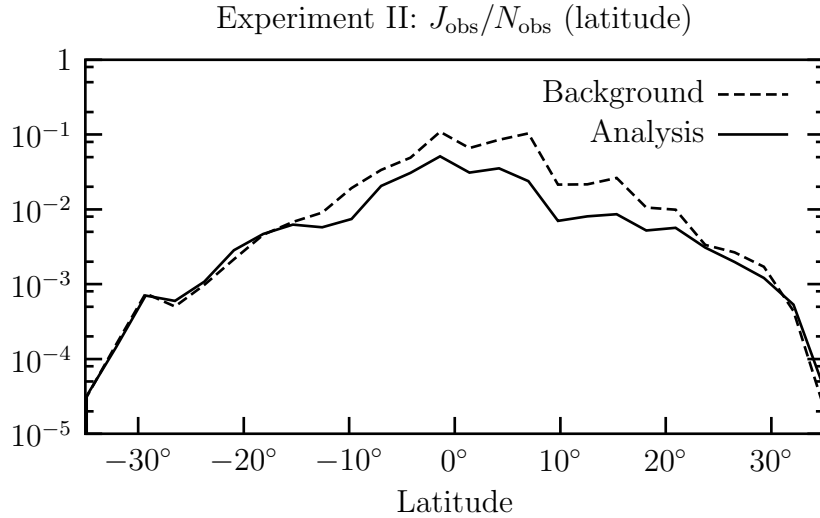


Figure 9: Experiment II. $J_{\text{obs}}/N_{\text{obs}}$ as a function of latitude on a logarithmic scale. N_{obs} is the number of observations in the assimilation window. Values are for the assimilation cycle 4, ending on April 9, 1995 (see Figure 3). The solid (dashed) line represents the run with (without) data assimilation, which is runA2 (runBG2).

assimilation. The final (fourth assimilation window, ending on April 9, 1995) total cost accounts 0.29 is for approximately 90% due to the misfits in the equatorial region, see Figure 9.

The differences in potential temperature for April 9, 1995 are in Figure 10. In the central equatorial Pacific ($10^{\circ}\text{S} - 15^{\circ}\text{N}$) a substantial reduction of the misfit is achieved (see also Figure 9). Thus, the 4DVAR method has skill in the equatorial wave guide. However, in other parts of the tropical Pacific the data assimilation does not result in an improved ocean model state. A comparison of all the panels of Figure 10 with those of Figure 6 confirms the expectation that the 4DVAR scheme is better suited for correcting the effects of wind-stress perturbation than of initial-state errors.

The wind-stress update (not shown) varies from zero to 25% of the first-guess wind stress, which is in agreement with the bounds of assumed standard deviation of the wind-stress error, discussed in section 3.

5 Assimilating real observations

In Experiment III the real XBT and buoy data in the region of 30°S to 30°N are assimilated for the 98 days considered. In this experiment, the data assimilation is counteracting errors in the initial state, the forcing and the ocean model.

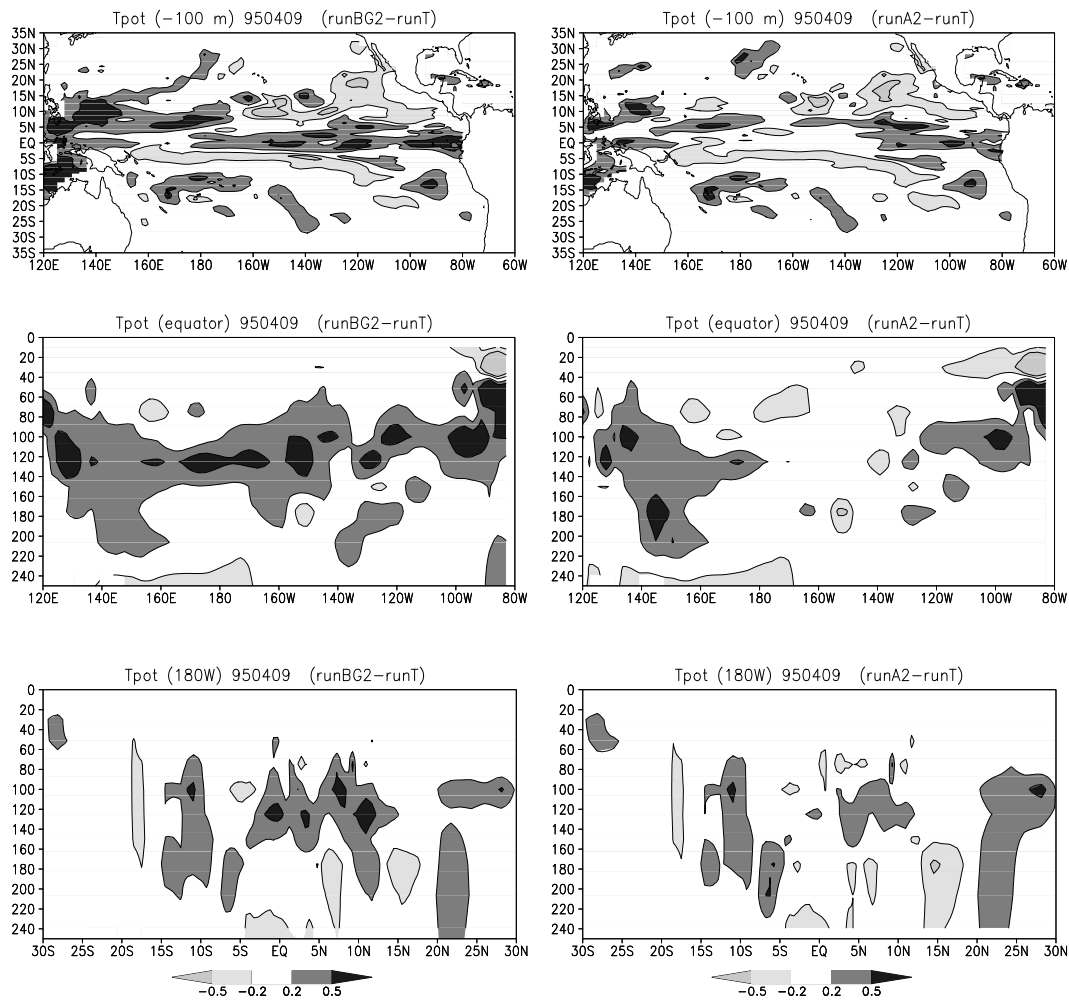


Figure 10: Experiment II: Potential-temperature differences (K) at the end of assimilation cycle 4 (April 9, 1995). The differences are between (left panels) the background run and the truth run and (right panels) between the analysis run (runA1) and the truth run. The 100 m layer differences are in the top panels. The differences along the equator and the 180°W meridian are in the middle and bottom panels, respectively. Data of the top layer are not included.

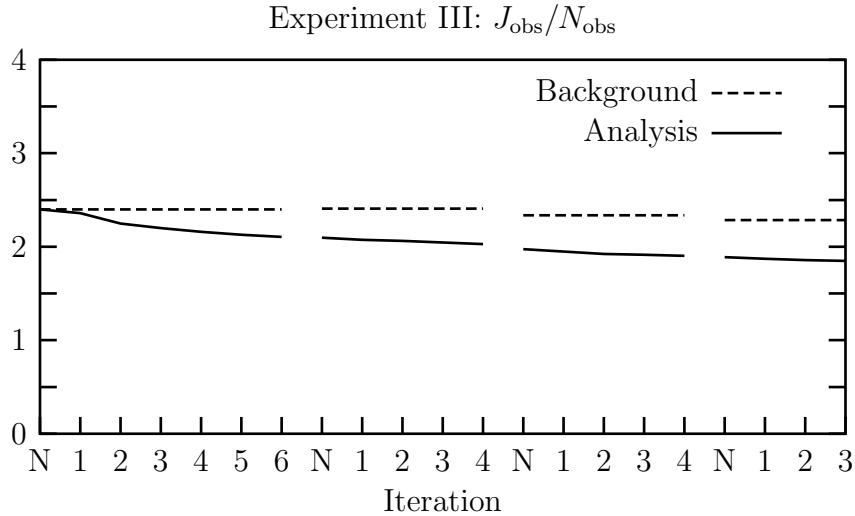


Figure 11: Experiment III. Convergence of $J_{\text{obs}}/N_{\text{obs}}$ as a function of iteration and assimilation cycle. N_{obs} is the number of observations in the assimilation window. The 4 cycles are the partly overlapping (see Figure 3) assimilation windows of 8 weeks. The solid (dashed) line represents the run with (without) data assimilation, which is runA3 (runBG3).

Therefore, the expected residuals are larger. The assumed standard deviation for the observation error is set to 1.0K (see section 3), because we do not expect that the model is able to come much closer to the observations in a realistic way. The results of the 4DVAR scheme are compared with those of the OI analysis of *Alves et al.* [1998]. Both the first-guess wind stress (EOA) and the initial state (from the ECMWFs OI analysis) are applied as given. The runs with and without data assimilation are runA3 and runBG3, respectively.

Again, we first consider the observational costs. These are depicted in Figure 11. The final value 1.84 differs from one, which is the expected value for perfect error estimates. A closer inspection of the distribution of the cost function reveals that this difference is partly caused by very large residuals for frequent observations in a few grid boxes. One example is the strong peak near 32°N in $J_{\text{obs}}/N_{\text{obs}}$ as a function of latitude (Figure 12). This peak is in fact located in one grid box at 135°E , 32°N (in the Kuroshio current), where two buoys give daily profiles (see Figure 1). The HOPE model representation of the Kuroshio is too wide and too shallow in this area due to the coarse grid. Consequently, the modeled thermocline in this grid box is approximately at 350 m, whereas in reality the thermocline is much deeper. A profile of the residuals is depicted in Figure 13. The largest residuals exceed 6 K. These residuals add up to 30% of J_{obs} . This model error leads to unrealistic wind-stress innovations in a wider area

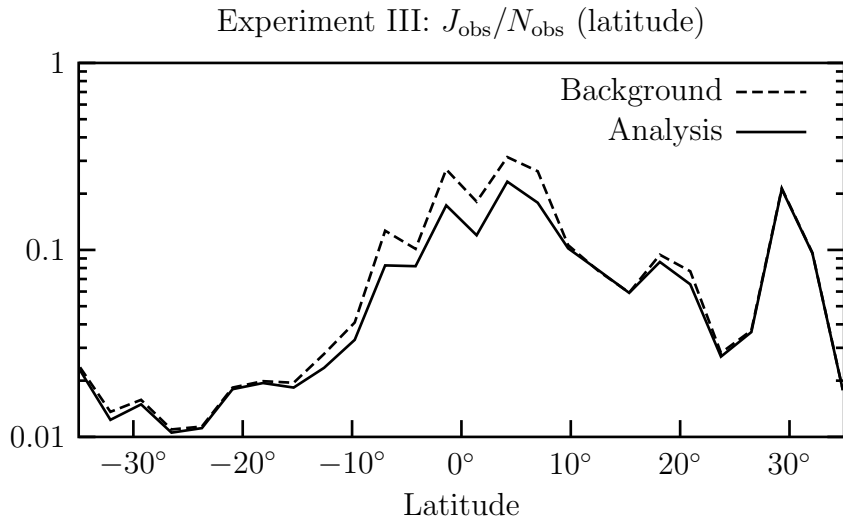


Figure 12: Experiment III. $J_{\text{obs}}/N_{\text{obs}}$ as a function of latitude on a logarithmic scale. N_{obs} is the number of observations in the assimilation window. Values are for the assimilation cycle 4, ending on April 9, 1995 (see Figure 3). The solid (dashed) line represents the run with (without) data assimilation, which is runA3 (runBG3).

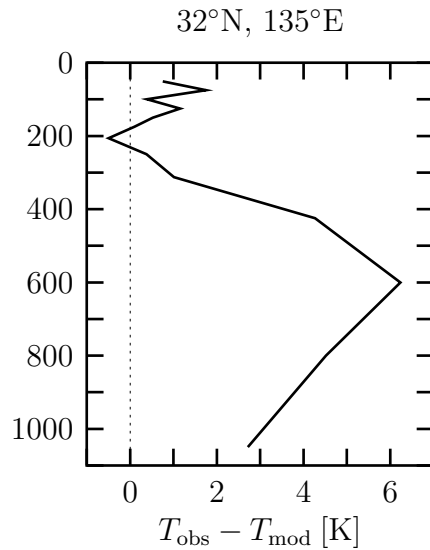


Figure 13: The averaged temperature residuals (observation–runA1) of the best-guess analysis of the last assimilation cycle in the grid box centered at 135°E, 32°N. The averaging is over the complete assimilation window. (The HOPE model has a thermocline that is much shallower than reality).

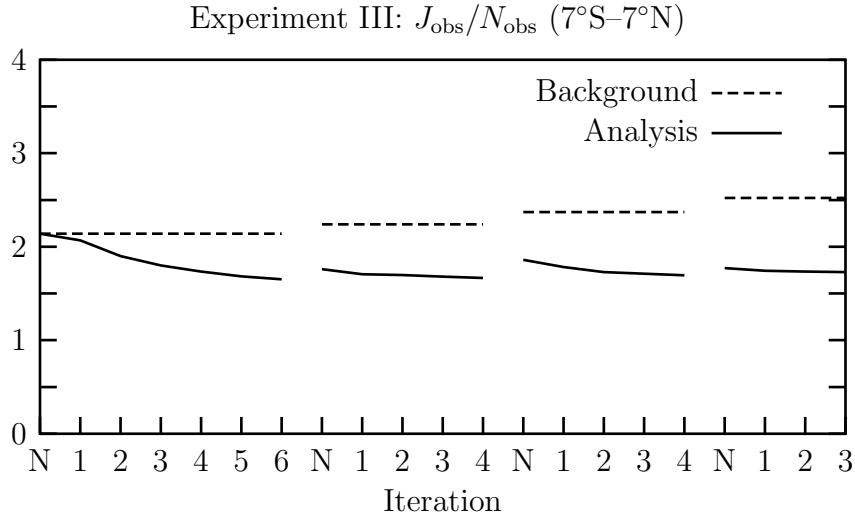


Figure 14: Experiment III. Convergence of $J_{\text{obs}}/N_{\text{obs}}$ between 7°S and 7°N as a function of iteration and assimilation cycle. N_{obs} is the number of observations in the assimilation window. The 4 cycles are the partly overlapping (see Figure 3) assimilation windows of eight weeks. The solid (dashed) line represents the run with (without) data assimilation, which is runA3 (runBG3).

around this point.

Another problematic spot is at 138°E , 7°N . Time series analyses of buoys in the vicinity (not shown) reveal a very strong January cold anomaly in the thermocline with a very sharp front between the cold and warm water. In this study, we assume a zonal decorrelation length $\lambda_x(x, y)$ of τ_x in the order of 5–7 grid boxes, (about 18°). This is too large to have an effect on structures of such a small scale. Thus, this kind of residual structures cannot be resolved.

The wind-stress response of the 4DVAR method to the large residuals is to make large updates. This affects the optimization process. In all the assimilation cycles, the background constraint J_{bg} becomes active in early stage of the assimilation. After a few iterations the number of function evaluations required by the M1QN3 routine increases very rapidly, while the achieved innovation is very marginal. This suggests that the optimization already approaches a (local) minimum. At this point, the continuation of the optimization becomes unreasonable, because the computational burden is very large. Therefore, we have halted the optimization, whenever M1QN3 requires more than three function evaluations per iteration. The break is after 4, 4, and 3 iterations for the second, third and fourth assimilation cycle, respectively.

Despite these difficulties, the convergence behavior for the equatorial Pacific (7°S – 7°N) is fairly similar to the experiment I and II (compare the Figures 14, 4

and 8). This suggests that the 4DVAR method has performed as expected from the identical-twin experiments.

Next we consider updates for the ocean-model state of April 1, 1995, eight days before the end of the fourth assimilation window. Figure 15 depicts the difference between the background (runBG3) ocean state with that of the OI scheme (left panels) and the 4DVAR state (right panels). In the equatorial region (roughly between 12°S and 12°N), the large-scale difference patterns are fairly similar among the two data-assimilation methods. This can be seen in the top, middle and bottom panels of Figure 15. However, the effects of the 4DVAR scheme are limited to the top 180 m in the central Pacific, along the equator (see middle right panel). Another dissimilarity between the methods is that the OI method resolves smaller scale structures. Some of these structure originate from isolated measurements. For example, in the layer between 120 m and 180 m depth several isolated anomalies can be seen (middle left panel of Figure 15) for the OI method, while 4DVAR update is much smoother for this layer.

In the other (off-equatorial) regions, the 4DVAR data-assimilation scheme does not have any impact, whereas the innovation of the OI method is large.

We also consider the wind-stress update (Figure 16). As in experiment II, the wind-stress update varies from zero to 20% of the first-guess wind stress (top panel). The wind-stress response is consistent with ocean-model physics. For example, the wind-stress update along the equator in the central Pacific (160°W to 120°W) enhances the trade winds. As a result, more warm water of the upper layers is pushed westward which results in the higher (lower) temperatures westward (eastward) of 145°W (see Figure 15, middle panel).

The wind-stress update has also been compared with the differences between the TAO observations and the ECMWF operational analysis that was used as the first guess. The latter has assimilated the TAO winds as if they had been measured at 10m, whereas the measurement height is in fact 4m, so the analyzed wind(stress) is lower than in reality. Along the equator the update indeed tends to compensate for this bias.

Finally, we compare the currents in the two assimilation schemes with observations. During this time the only TAO data that can be compared with the model are from the buoy at EQ, 140°W with current meters at 10m, 25m, 45m, 80m, 120m and 200m. In Figure 17 (top-left) the u measurements are shown for the first three months of 1995. The top-right panel gives the first-guess values for this period. In the bottom-left and bottom-right panels, the results of the 4DVAR and OI assimilation are plotted, respectively. The model always underestimates the strength and the depth of the undercurrent. Compared to the first guess, the 4DVAR data assimilation increases the strength of the undercurrent during this period. The agreement with the TAO observations is better than in the OI run, which has weaker currents. Further research is needed to show whether this is a

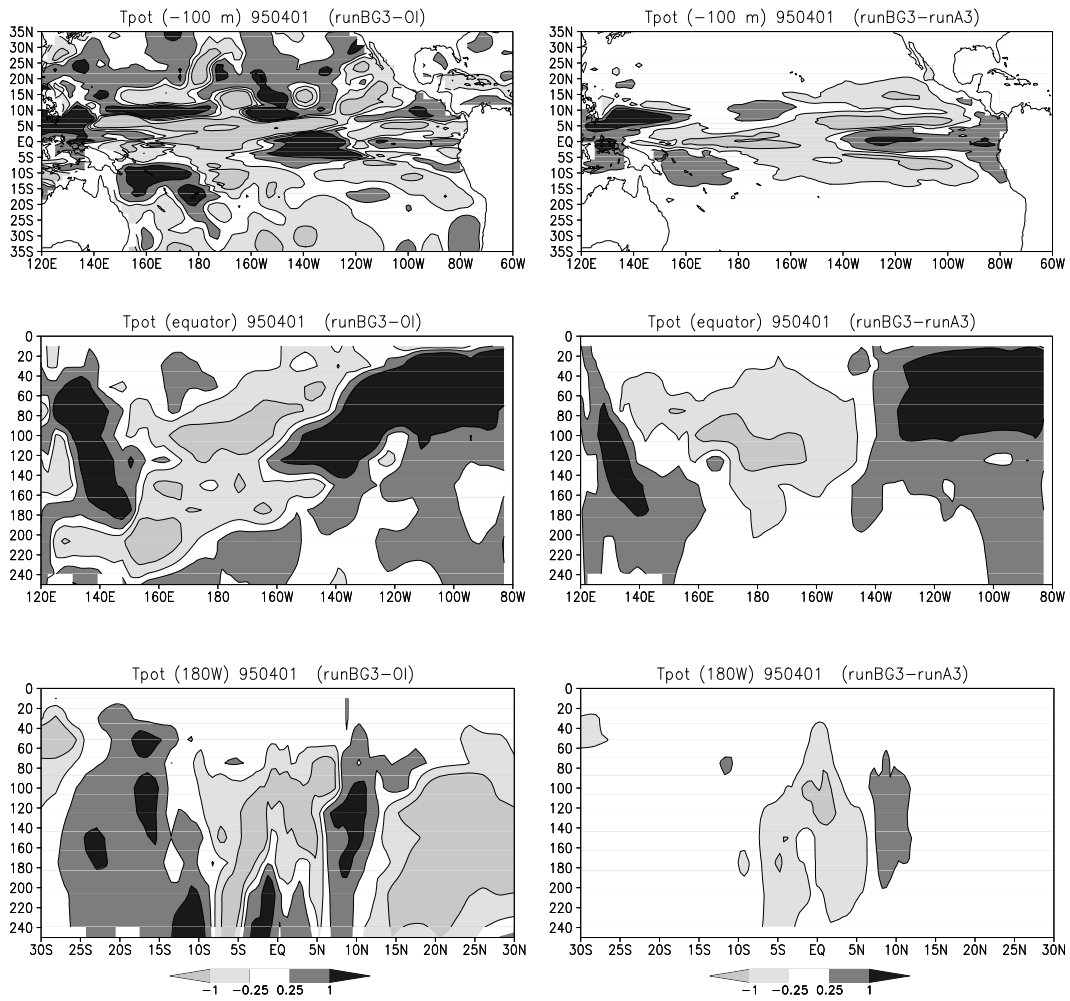


Figure 15: Experiment III: Potential-temperature differences (K) at April 1, 1995 (near the end of fourth assimilation cycle). The differences are between (left panels) the background run and the analyzed state by the Optimal Interpolation scheme, and (right panels) between the background run and the 4DVAR assimilation run. The 100 m layer differences are in the top panels. The differences along the equator and the 180°W meridian are in the middle and bottom panels, respectively. Data of the top layer are not included.

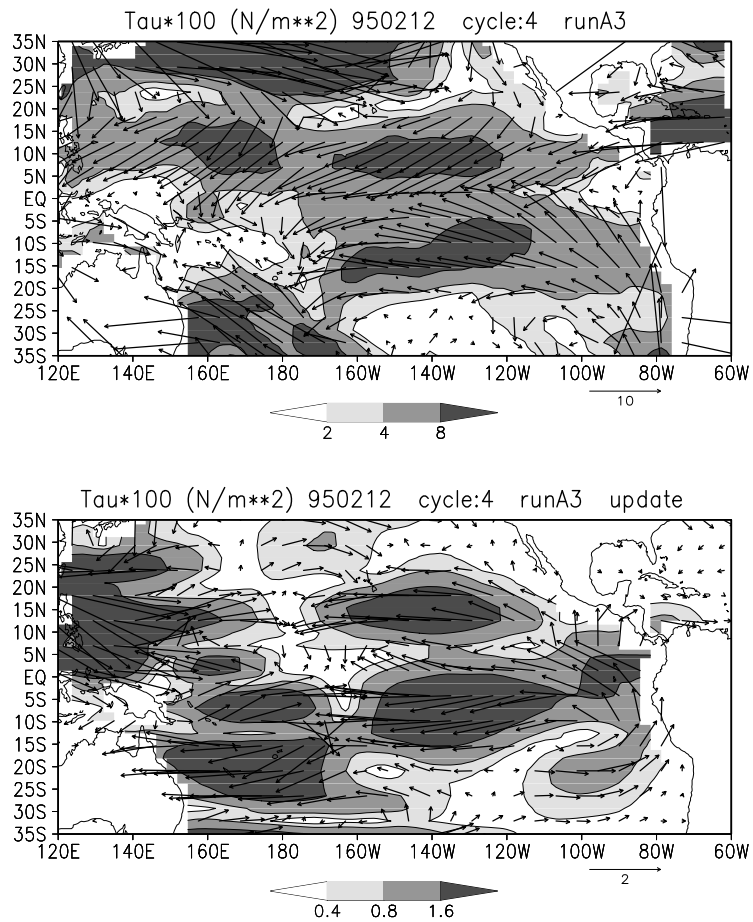


Figure 16: Experiment III: (top panel) first-guess wind stress and (bottom panel) update of wind stress by data assimilation. The plots are weighted time averages for the first week of the last assimilation cycle (i.e. February 12–18, 1995, see Figure 3). The weighting is according to the linear interpolation of equation 2. Note the different scaling of the panels.

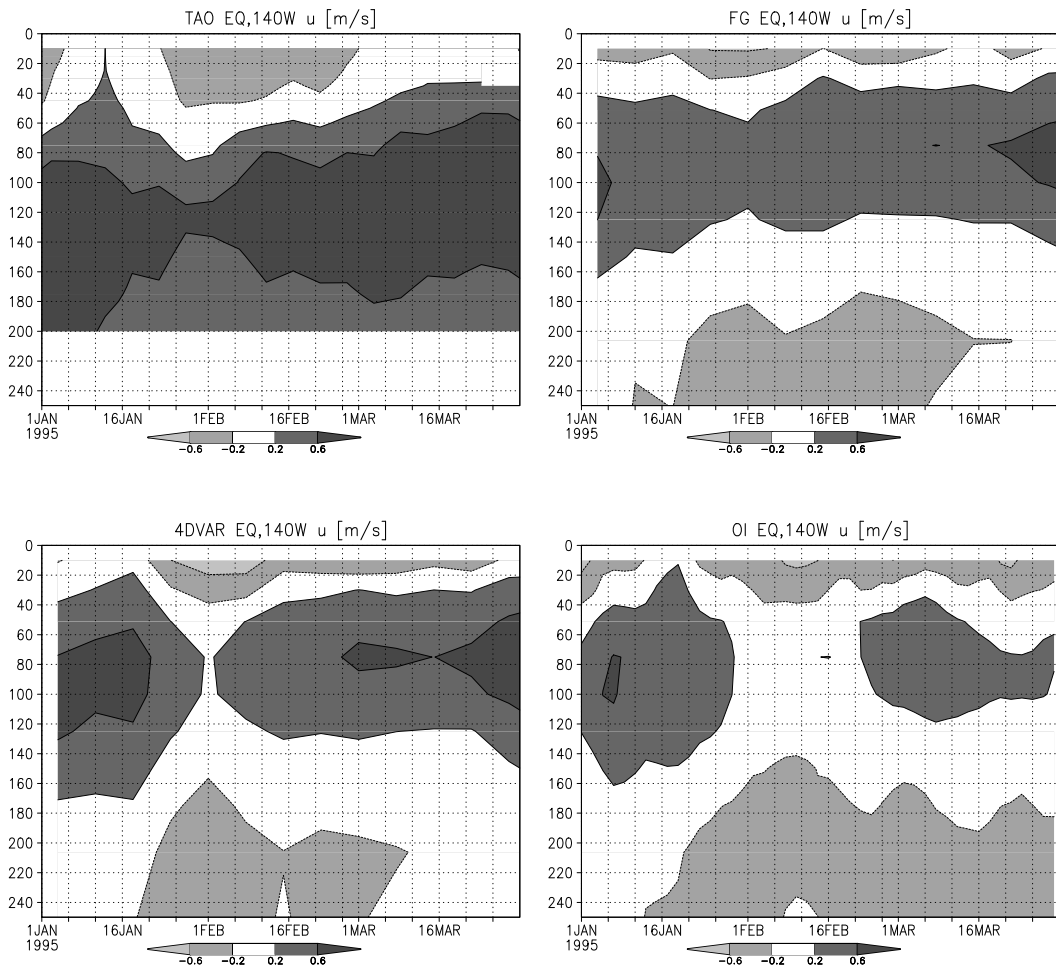


Figure 17: Zonal currents at EQ,140°W in early 1995. Top-left: 5-daily TAO current meters at 10m, 25m, 45m, 80m, 120m and 200m. Top-right: weekly first-guess values. Bottom-left: weekly values in the 4DVAR experiment III. Bottom-right: two-daily values in the OI assimilation.

consistent feature of this 4DVAR data assimilation scheme.

6 Discussion

6.1 Efficacy

The experiments of the previous sections have shown that the relevant innovations of both the wind stress and upper-ocean temperatures are confined to the Equatorial Pacific (10°S – 10°N). In the off-equatorial regions the innovation in wind stress is not necessarily zero, but the effects on the ocean-model analysis are small. Therefore, the performance of the method in the equatorial and the off-equatorial regions are discussed separately. There are two reasons for the good performance of the 4DVAR method in the equatorial region. These reasons are not independent. The first reason is that disturbances in the upper ocean are guided along the equator. The most important example are Kelvin waves. Kelvin waves are triggered by wind-stress variations near the equator and travel eastward with a phase speed of about $2 - 3 \text{ ms}^{-1}$. This means that many locations can be reached within an eight-week period. The upper ocean temperature differences (residuals) associated with these waves are translated into changes to the observational cost. The 4DVAR method propagates this information backward in time to make the appropriate equatorial wind-stress innovations and hence the desired innovations to the ocean model trajectory.

The second reason is simply the availability of a dense, uniformly distributed observational network that assures that (propagating) disturbances are indeed observed and translated into a substantial contribution to the observational cost. 70% of the total number of observations are located between 10°S and 10°N and these dominating the cost function (see Figures 5, 9 and 12). In fact, one of the prime goals of TAO array is to observe the equatorial trapped wave activity. In an eight-week period a fast Kelvin wave will pass at least 6 lateral TAO arrays.

In the off-equatorial region (outside 10°S – 10°N) the 4DVAR using wind stress control is not very effective (see e.g. the top and bottom panels of Figure 15). In this case, both reasons of the good performance in the equatorial region are lacking. Disturbances are propagated by higher-order Rossby waves. However, the speed of these waves is an order of magnitude smaller than that of Kelvin waves. Therefore, a very dense network is required for wind stress to have a significant impact on sub-surface observations. In reality, the number of observations in the off-equatorial regions is low and the denser coverage is confined to coastal areas where most of the ship tracks are located, see Figure 1.

6.2 Optimality

A remaining question is the optimality of 4DVAR data assimilation. Many parameters in the current configuration of the 4DVAR method are from motivated guesses. This implies that some modifications might lead to an improved performance. Some of the modifications are technical, others may have a more physical nature. For instance, in subsection 4.1, it was noted that after data assimilation there still is an observational cost J_{obs} (mainly due to equatorial residuals) of 7% of the background value. This value might be lowered with a modification of e.g. the length of assimilation window. To clarify this further studies are needed, possibly with some withheld observed data to have an independent measure for the improvements. This is beyond the scope of this article. Instead, we will discuss some general properties of important parameters in more detail.

Firstly, an essential aspect of any 4DVAR system is the proper modeling of the error covariances. Experiments I, II and III have shown that the assumed magnitude of errors in wind stress and upper ocean temperature are reasonably in balance. For example, in experiment III, the background term constraints the wind-stress innovations when the related residuals are too large as a result of model deficiencies. However, the current guess of the decorrelation lengths may be somewhat large, in particular $\lambda_x(x, y)$ of τ_x , see Figure 2. An additional analysis run has been made for experiment I but with $\lambda_{x,y}(x, y)/2$ for both τ_x and τ_y . This run (not shown) results indeed in larger corrections on smaller scales and hence in an improved ocean analyses. In this case, the observational cost after data assimilation is 5% of the background value (instead of 7%). However, care should be taken not to create new difficulties with too small decorrelation lengths, such as mutually compensating wind-stress innovations in adjacent grid boxes and a cost function with many local minima.

Secondly, an obvious way to improve the 4DVAR method is to enlarge the assimilation window. An improved performance in the equatorial regions can be expected for the same reasons as discussed in the previous subsection. However, this would increase the computational burden considerably. To have an impact in the off-equatorial region the assimilation window should be extended to several months or even years.

Thirdly, the quadratic shape of the cost function might be reconsidered. Experiment III has demonstrated that large localized ocean model errors, like in the Kuroshio, can have an undesired large effect on the data assimilation and hence the ocean analysis. Solutions to problems of this kind are to ignore some observations or to introduce a more tailored weighting of large residuals. For example, a multiplication factor $1/(1 + (|T_{\text{res}}| - 5)^2)$ can be employed for discarding temperature residuals T_{res} larger than 5 K [e.g. *Behringer et al.*, 1998].

Finally, we address some aspects of the minimization. The re-use of wind-

stress control in consecutive assimilation windows has proven to be beneficial. For example, the low observational cost in the second assimilation window of Figure 4 could not have been achieved with a restart of the minimization from the first-guess wind stress. Most of the feasible reduction is obtained in less than 5 iterations. Another aspect is globality of the minimum. In general, it is hard to prove that the best-guess wind stress is the global minimizer. However, it is likely that our updates are for the global optimum, because our first-guess wind stresses are realistic and the cost function is a fairly smooth functions of the control.

6.3 Comparisons and possible extensions

It is interesting to compare the performance of this 4DVAR scheme with other data-assimilation techniques and other ocean models. In experiment III, a first comparison is given between the OI and 4DVAR method (see Figure 15). In the equatorial region the large-scale innovation of the OI and 4DVAR method are remarkably similar. For the off-equatorial regions the wind stress adjusting 4DVAR method is not yet an alternative.

The 4DVAR scheme of this study is implemented for all the HOPE surface forcings over the global ocean. Therefore, natural extensions are 1) to include the heat (and possibly the freshwater flux) in the experiments and 2) to assimilate ocean observations globally. The adjustment of the heat flux requires additional considerations with respect to the SST relaxation which is also adjusting the effective heat flux. An additional cost term for the SST observations can be introduced to replace the relaxation term. The results of experiment III in the off-equatorial regions indicate that expectations with respect to the innovation of global forcing and upper ocean fields should be moderate. Current ocean observations are still too sparse for a feasible length of assimilation window.

A very promising way forward is to combine initial-state and surface-forcing control in the 4DVAR method. In this way, the advantages of both approaches of control can be exploited and the initialization and forcing errors can be considered more individually. However, before we get into this stage, more direct comparisons with 4DVAR methods controlling the initial state are needed to assess the merits and drawbacks of the surface forcing control in further detail. *Weaver and Vialard* [1999] have developed an incremental 4DVAR method that controls the initial state in the tropical Pacific. They use a different OGCM, but the same observational data set. It would be interesting to compare our results with those of *Weaver and Vialard* [1999] for an agreed time period and region in the equatorial Pacific. A relevant and objective test of comparing ocean 4DVAR methods would be the predictive skill of a coupled model with the same atmosphere model.

Finally, another promising way forward is the assimilation of other observational data. Obvious candidates are satellite altimeter data and salinity measurements. *Katz et al.* [1995] have shown that sea level observation of the

TOPEX/Poseidon satellite are a good proxy for the dynamical height in the tropical ocean. The density of altimeter measurements is high, which means that also off-equatorial regions in the tropical Pacific can be sampled, because more locations can be influenced by observations within an eight-week period. Other studies [e.g. *Cooper, 1988; Vossepoel and Behringer, 1999*] demonstrate that assimilation of salinity and altimeter data improves analysis of the salinity variability, which has an appreciable impact on the density distribution in the upper ocean [*Lukas and Lindstrom, 1991*]. In a variational approach, the inclusion of these data is straightforward.

7 Conclusions

A 4DVAR data assimilation scheme that adjusts the ocean-surface forcing of a OGCM has been implemented for the HOPE OGCM. Two identical-twin experiments and an experiment with real observation show that adjusting wind stress with the 4DVAR scheme is an effective way to correct errors in the upper ocean analysis and in the wind stress over the tropical ocean.

The re-use of wind stress control in consecutive assimilation windows results in a good convergence of the 4DVAR scheme with a limited number of cost function evaluations.

In the equatorial Pacific, a large reduction in wind-stress and upper-ocean temperature misfits can be achieved using an assimilation window of eight weeks. The main reason is that the equatorial region combines a high ocean-model sensitivity to short term disturbances with a high number of observations which are uniformly distributed. In off-equatorial regions of the Pacific this combination is lacking and the performance of the 4DVAR method is not that well.

Improvements of the efficacy in both the equatorial and off-equatorial regions are expected from longer assimilations windows and new estimates of the wind stress error covariances.

Acknowledgments

We are grateful to the Seasonal Forecasting Group of the ECMWF for their support and collaboration. We also thank Gerbrand Komen for his valuable comments on this article. This work was supported by the Dutch National Research Programme on Global Air Pollution and Climate Change under contract no. 951207 and by the Geosciences Foundation (GOA) of the Netherlands Organization of Scientific Research.

References

- Alves, J. O., D. L. T. Anderson, T. N. Stockdale, M. A. Balmaseda, and J. Segschneider, Sensitivity of ENSO forecasts to initial conditions, *Proceedings of the Triangle 1998 Symposium*, 207–233, 1998.
- Anderson, D. L. T., J. Sheinbaum, and K. Haines, Data assimilation in ocean models, *Rep. Prog. Phys.*, *59*, 1209–1266, 1996.
- Behringer, D. W., M. Ji, and A. Leetma, An improved coupled model for ENSO prediction and implications for ocean initialization. Part I: the ocean data assimilation system., *Mon. Weath. Rev.*, *126*, 1013–1021, 1998.
- Bryden, H. L., New polynomials for thermal expansion, adiabatic temperature gradient and potential temperature gradient of sea water, *Deep-Sea Res.*, *20*, 401–408, 1973.
- Cane, M. A., A. Kaplan, R. N. Miller, B. Tang, E. Hackert, and A. J. Busalacchi, Mapping tropical pacific sea level; data assimilation via a reduced state space Kalman filter, *J. Geophys. Res.*, *101*, 20345–22617, 1996.
- Cooper, N. S., The effect of salinity in tropical ocean models, *J. Phys. Oceanogr.*, *19*, 697–707, 1988.
- Courtier, P., J.-N. Thépaut, and A. Hollingsworth, A strategy for operational implementation of 4D-Var, using an incremental approach, *Quart. J. Roy. Meteor. Soc.*, *120*, 1367–1387, 1994.
- Egbert, G. D., A. F. Bennett, and M. G. G. Foreman, Topex/Poseidon tides estimated using a global inverse model., *J. Geophys. Res.*, *99*, 24821–24852, 1994.
- Gibson, R., P. Kållberg, S. Uppala, A. Hernandez, A. Nomura, and E. Serrano, The ECMWF re-analysis project report series. 1. ERA description, ECMWF, Reading, UK, 1997.
- Gilbert, J. C., and C. Lemaréchal, Some numerical experiments with variable-storage quasi-newton algorithms, *Math. Program B*, *45*, 407–435, 1989.
- Ji, M., and A. Leetma, Impact of data assimilation on ocean initialization and El Niño prediction, *Mon. Weath. Rev.*, *125*, 742–753, 1997.
- Katz, E. J., A. Busalacchi, M. Bushnell, F. Gonzalez, L. Gourdeau, and M. McPhaden, A comparison of the ocean surface height by satellite altimeter, mooring and inverted echo sounder., *J. Geophys. Res.*, *100*, 25101–25108, 1995.
- Levitus, S., *Climatological atlas of the World Ocean*, 173 pp., NOAA Prof. Pap. no. 13, U. S. Gov. Print. Office, Washington, D. C., 1982.
- Lukas, R., and E. R. Lindstrom, The mixed-layer of the western equatorial Pacific, *J. Geophys. Res.*, *96*, 3343–3357, 1991.
- Malanotte-Rizzoli, P. (Ed.), *Modern Approaches to Data Assimilation in Ocean Modeling*, 455 pp., Elsevier, Amsterdam, 1996.

- McPhaden, M. J., Genesis and evolution of the 1997-98 El Niño, *Science*, **283**, 950–954, 1999.
- McPhaden, M. J., A. J. Busalacchi, R. Cheney, J. R. Donguy, K. S. Gage, D. Halpern, M. Ji, P. Julian, G. Meyers, G. T. Mitchum, P. P. Niiler, J. Picaut, R. W. Reynolds, N. Smith, and K. Takeuchi, The Tropical Ocean Global Atmosphere (TOGA) observing system: a decade of progress, *J. Geophys. Res.*, **103**, 14169–14240, 1998.
- Miller, R. N., and M. A. Cane, Tropical data assimilation: Theoretical aspects, in *Modern Approaches to Data Assimilation in Ocean Modeling*, edited by P. Malanotte-Rizzoli, pp. 207–233, 1996, Elsevier, Amsterdam, 1996.
- Oldenborgh, G. J. van, G. Burgers, S. Venzke, C. Eckert, and R. Giering, Tracking down the ENSO delayed oscillator with an adjoint OGCM, *Mon. Weath. Rev.*, **127**, 1477–1496, 1999.
- Reynolds, R. W., and T. M. Smith, A high resolution global sea surface temperature climatology, *J. Climate*, **8**, 1571–1583, 1995.
- Sheinbaum, J., and D. L. T. Anderson, Variational assimilation of XBT data. Part I, *J. Phys. Oceanogr.*, **20**, 672–688, 1989.
- Stockdale, T. N., Coupled ocean atmosphere forecast in the presence of climate drift, *Mon. Weath. Rev.*, **125**, 809–818, 1997.
- Stockdale, T. N., A. J. Busalacchi, and D. E. Harrison, Ocean modeling for ENSO, *J. Geophys. Res.*, **103**, 14325–14355, 1998.
- Tziperman, E., and K. Bryan, Estimating global air-sea fluxes from surface properties and from climatological flux data using an ocean general circulation model, *J. Geophys. Res.*, **98**, 22629–22644, 1993.
- Vossepoel, F. C., and D. W. Behringer, Impact of sea level assimilation on salinity variability in the western equatorial Pacific, *J. Phys. Oceanogr.*, *in press*, 1999.
- WCRP, Scientific plan for the Tropical Ocean Global Atmosphere program, *WMO/TD-64*, 146 pp., World Climate Research Program, Geneva, 1985.
- Weaver, A. T., and D. L. T. Anderson, Variational assimilation of altimeter data in a multilayer model of the tropical Pacific ocean, *J. Phys. Oceanogr.*, **27**, 664–682, 1996.
- Weaver, A. T., and J. Vialard, Development of an ocean incremental 4D-var scheme for seasonal prediction, *Proceedings of Third WMO International Symposium on Assimilation of Observations in Meteorology and Oceanography*, 207–233, 1999.
- Wolff, J.-O., E. Maier-Reimer, and S. Legutke, The Hamburg Ocean Primitive Equation model HOPE, *DKRZ Tech. Rep. No. 13*, Deutsches Klimarechenzentrum, Bundesstr. 55, D-20146 Hamburg, Germany, Hamburg, 1997.
- Yu, L., and J. J. O’Brien, Variational data assimilation for determining the seasonal net surface heat flux using a tropical Pacific ocean model, *J. Phys. Oceanogr.*, **25**, 2319–2343, 1995.

Zebiak, S. E., and M. A. Cane, A model of El Niño–Southern Oscillation, *Mon. Weath. Rev.*, 115, 2262–2278, 1987.